Alterations in Fiber Pathways Reveal Brain Tumor Typology: a Diffusion Tractography Study

Conventional structural Magnetic Resonance (MR) techniques can accurately identify brain tumors but do not provide exhaustive information about the integrity of the surrounding/embedded white matter (WM). In this study, we used Diffusion-Weighted (DW) MRI tractography to explore tumor-induced alterations of WM architecture without any a priori knowledge about the fiber paths under consideration. We used deterministic multi-fiber tractography to analyze 16 cases of histologically classified brain tumors (meningioma, low-grade glioma, high-grade glioma) to evaluate the integrity of WM bundles in the tumoral region, in relation to the contralateral unaffected hemisphere. Our new tractographic approach was able to properly evaluate the type and severity of WM involvement which strongly correlated with the histopathological features of the tumor ($r=0.83$, $p=0.0001$). Moreover, the amount of affected fiber tracts were significantly ($p=0.0006$) different among tumor types. Our approach proposes a new role for diffusion tractography in the detection of tumor aggressiveness in those critical cases in which the lesion does not involve any major/known WM paths and a priori information about the local fibers' anatomy is lacking.

Alterations in Fiber Pathways Reveal Brain Tumor Typology: a Diffusion Tractography Study

Characterization of White Matter Damage

Martina Campanella, PhD [1,*], Tamara Ius, MD [1,2], Miran Skrap, MD[2] , Luciano Fadiga, PhD [1,3]

[1] Department of Robotics, Brain and Cognitive Sciences, Istituto Italiano di Tecnologia, Genoa, Italy

[2] Department of Neurosurgery, Az. Ospedaliero-Universitaria Santa Maria della Misericordia, Udine, Italy

[3] Section of Human Physiology, University of Ferrara, Italy

*Corresponding author:

Martina Campanella, PhD

Department of Robotics, Brain and Cognitive Sciences

Istituto Italiano di Tecnologia

Via Morego 30, 16163, Genoa, Italy

Phone: +39 010 71781420

Fax: +39 010 717081

e-mail: martina.campanella@iit.it

Introduction

A number of brain pathologies affect white matter (WM) fiber pathways, either by disruption, infiltration or displacement [1,2]. Knowledge of such alterations may provide useful information during neurosurgery, particularly in the case of infiltrating lesions, where the extent of excision and the prognosis are positively correlated[3,4]. In fact, while highly aggressive lesions significantly impair the morphology and functionality of infiltrated WM, less aggressive tumors may simply displace the surrounding brain structures. These differing behaviors influence surgical strategy, mainly aimed at finding the best compromise between amount of removal and preserved brain functionality.

Nowadays, advanced techniques such as diffusion tensor imaging (DTI) allow for non-invasive tracking of fiber bundles characterized by a well-known hodology and course (e.g. the corticospinal system). The task becomes however more difficult when a priori information about the anatomy of the local fibers is lacking.

DTI[5] is based on the fact that water diffusion is greater along a fiber's main axis rather than perpendicularly to it and can be used to estimate fiber orientation in each MR voxel. Tractography uses this local information from the reconstructed diffusion tensors to identify global white matter tracts [6-8]. Over the last decade, diffusion MRI has often been used to investigate WM alterations. Clinicians have gained useful insights from these studies for surgical planning[9,10] and assessing reorganization after injury[11-12] or specific therapy[13]. Several reports have assessed damage to fiber tracts in relation to cerebral neoplasm types using DTI metrics, such as fractional anisotropy (FA) and mean diffusivities (MD) [14-17]. The majority of those works were based on a priori anatomical knowledge about fiber courses and use known anatomical landmarks to select seed regions and to reconstruct major fiber tracts[18-22].

However, WM mapping based on known normal anatomical locations as seeds might be

misleading, since the WM architecture can be deviated from its normal location and edema can mask the path of fiber tracts. A complementary approach to increase precision is to integrate fMRI information[23,24] or Intraoperative Electrical Stimulation (IES)[25] data with tractographic data. IES is however invasive and can be performed only during surgery and not during surgical planning. Moreover, it should be taken into account the possible alteration of the functional responses, both for fMRI and IES, induced by the tumor[26].

Since the diffusion tensor model infers the orientation of one single fiber per voxel, the DTI approach is only able to trace major tracts in the brain and cannot model complex WM architectures. Several approaches have recently been proposed to overcome this limitation and to estimate multiple fiber directions within the same voxel [27-29]. One of such techniques, Persistent Angular Structure (PAS)–MRI[30], starts from an economical spherical acquisition paradigm and computes a function of the sphere that reflects the angular structure of the water molecules displacement density by using the peaks of this function as fiber-orientation estimate. This particular method ensures higher sensitivity to fiber crossings.

Here, we propose a novel approach to assess fiber displacement/disruption caused by brain lesions by using deterministic tractography from High Angular Resolution Diffusion (HARD) data[31] acquired from patients affected by histologically characterized gliomas or meningiomas. PAS-MRI was adopted and, after reflecting on the contralateral normal hemisphere the site of the lesion and using this new location as seed region, all possible distinct bundles and trajectories of tumor-involved WM tracts were evaluated in relation to the myeloarchitecture, without any atlas-guided tract reconstruction. By this approach we have been able to identify fiber bundles which would have presumably run through the tumor and the estimated fiber bundles were first flipped-back and then compared to the altered tracts of the lesioned hemisphere.

We evaluated the capability of our technique capability to determine the typology and aggressiveness of the lesion by analyzing the relationship between the severity of tumor-induced damages and lesion-specific histological features. In particular, we studied the differences in the alterations of fiber pathways between the two types of lesions considered, meningioma and gliomas. We tested the method by characterizing the degree of WM alteration according to their MIB-1 labeling indexes[32], a monoclonal antibody expression of the percentage of positive staining tumor cell nuclei. We used deterministic tractography as a straightforward, rapid technique but we also performed probabilistic tractography[33,34], incorporating all the diffusion information in order to obtain a measure of uncertainty and to evaluate the results of our tracking procedure. The analysis confirmed that the deterministic algorithm reconstructs all the important connections.

Material and Methods

Patient Information

Sixteen patients diagnosed with brain tumors were considered for the study (9 males, 7 females), aged from 27 to 68 years, with a mean age of 42.62 ± 10.72 years (Table 1). Lesions included meningiomas in five patients (Cases M #1-5), low-grade gliomas in seven patients (Cases LGG #1-7), and high-grade gliomas in four patients (Cases HGG #1-4). Lesions were classified on the basis of tumor histological features as determined by biopsy and according to the World Health Organization (WHO) criteria[35]. The MIB-1 index was also calculated, and it ranged from 2 to 35%. This study was approved by the local institutional ethics committee on human research of the University Hospital Santa Maria della Misericordia of Udine and clinical data were acquired following the guidelines of the Department of Neurosurgery. Informed consent was obtained

from all the patients who participated in this clinical investigation.

Imaging Protocol

Diffusion-weighted MRI data were obtained on a 3T scanner (ACHIEVA 3T, Philips, Netherlands) using a multi-shot DWI-SE sequence (FOV: 240x240x105mm; voxel 1.0×1.0×1.5mm; 70 slices acquired parallel to the line connecting the anterior commissure to the posterior commissure, no slice gap; TE=74.8ms; TR=8833ms; NEX=1; parallel reconstruction). Diffusion weightings were isotropically distributed over 64 directions with a b value of 1000 s*mm^{-2}, for a total acquisition time of approximately 15 min. The MRI sessions also included T1-weighted (3D turbo-gradient-echo sequence, voxel size: 1.000x1.000x1.000 mm; 240 slices) and a Gadolinium-enhanced T1-weighted anatomical MR imaging (3D sagittal-turbo-flash sequence with TR=2300ms, TE=2860ms, IR=1100ms, flip angle=20°; voxel size: 1.000x1.000x1.000 mm; 240 slices, no gap between slices) was acquired, as well.

Data Analysis

Data analysis was carried out using the Camino software package[36] (www.camino.org.uk), FSL[37] (http://www.fmrib.ox.ac.uk/fsl), AFNI[38] (http://afni.nimh.nih.gov/afni), and ITK-SNAP [39], as follows.

Preprocessing.

DTI scans were first re-aligned for Eddy current-induced geometric distortions and head motion correction using affine registration to the first unweighted volume[40]. Skull-stripping was then performed using BET [40].

Both anatomical T1-weighted scans were rigidly registered to the individual diffusion spaces using the unweighted b0-image to estimate the transformation parameters (Linear Image Registration Tool, FLIRT, [41]).

Direction reconstruction.

A multi-fiber reconstruction approach was followed[42] and the PAS functions[30] were computed for each voxel. A reduced encoding approach was adopted [43], setting the number of basic functions in the PAS representation equal to 16. The local maxima of the PAS function corresponding to the three principal directions (PDs) were extracted for every voxel using the peak-finding algorithm implemented in the sfpeaks module of the Camino toolkit [36].

Seed.

For each patient, a 3D tumoral region of interest (ROI) was manually defined by precisely tracing the contours of the tumor mass slice-by-slice (www.fmrib.ox.ac.uk/fsl/) on the MRI images. Before a ROI was drawn, the unenhanced and enhanced acquired volumes were both inspected so that non-tumor tissue and large vessels were avoided. Subsequently, the ROI was mirrored across the sagittal mid-plane by a procedure included in the ITK-SNAP package[39] to obtain the homologous region in the healthy hemisphere. A segmentation framework, based on a modified Gaussian mixture model as implemented in SPM[44], was performed, and the white matter mask of the whole brain was identified. We computed the intersection between the mirrored tumor mask and the white matter one using the voxel-by-voxel arithmetic calculations included in the AFNI software package[38]. The intersection ROI was then transformed from the structural to the native diffusion space with a rigid-body registration, using the b0 image as a

reference[40]. In order to maintain the volume of the lesion and of the homologous region as faithful as possible to those in the native brain images, after the transformation, the masks were conservatively thresholded at 0.9. Lastly, all the co-registered ROI were visually checked for precision. The homologous ROI was used as the "seed" in the tractography analysis (Figure 1: a, b, c).

Tracking.

We employed a deterministic streamline tracking algorithm[45], modified in order to take into account multiple directions per voxel[42]. Streamlines were generated from every point within the seed mask in the healthy hemisphere. The tracking algorithm starts the same number of fibers as the number of PAS peaks in each seed voxel. An anisotropy value less than 0.2, a curvature of the streamline by more than 60 degrees across a voxel, and entrance of the streamline into an out-of-brain voxel were used as stopping criteria.

Target Generation.

The last ten voxels of each estimated fiber tract were taken into account. Since the main interest concerned the farthest projections in order to investigate the long- and medium-range connectivity alterations, an exclusive mask correspondent to the tumor region and its proximity (2 cm around) was created[39] and used to exclude voxels directly neighboring the seed region by means of AFNI voxel-by-voxel arithmetic modules[38]. The resulting dataset of voxels was visually inspected for their correspondence with the reconstructed tracks in order to estimate the number of clusters. A k-means clustering algorithm developed in-house was applied to identify the specific centroids towards groups of fibers from the seed projected. When fibers projected to two diametrically opposed brain areas, two centroids, one for each area, the ones reached by most of

the tracked pathways, were taken into account. In cases where fibers projected from the seed to nearby brain areas, only the centroid reached by most of the projections was considered. Subsequently, since there are asymmetric tracts in the human brain[46], a rather wide ROI (10mm-diameter sphere) around each defined centroid of interest was drawn[39] in order to ensure the reconstruction of all likely fiber tracts in both hemispheres. The corresponding target regions were so obtained.

Tracts of interest.

In four cases (Cases M3, M4, LGG1, and LGG5) two target regions were taken into account for the comparative tractography analysis. Afterwards, the WM bundles connecting the two selected target ROIs were investigated to estimate the contralateral fiber tracts which would have presumably run through the tumor. For this purpose, another tracking framework was implemented: once again, we ran deterministic tractography to generate streamlines from every point within the brain mask, this time used as the "seed". The same stop criteria previously described were adopted. Thereafter, the two target ROIs, previously identified, were applied as endpoint masks and the streamlines connecting them were reconstructed in the healthy hemisphere[47]. Finally, the target regions were sagittally mirrored and the tracts of interest in the affected hemisphere generated in the same manner as described above for the healthy hemisphere (Figure 1: d1, e1).

In the other twelve cases (Cases M1, M2, M5, LGG2, LGG3, LGG4, LGG6, LGG7, and HGG #1-4) only one target region was considered. The homologous region mask was dilated by a factor of 1.2 to study the fibers in the proximity of the lesion as well, applying the dilation

mathematical morphology procedure implemented in ITK-SNAP. A new homologous ROI was so created. Hence, in the healthy hemisphere, the streamlines connecting the dilated ROI and the target were tracked to estimate the contralateral WM tracts involved in the tumor area. The procedure and the tracking parameters were the same as those adopted in the previous case: first, all the fibers generated in the brain volume were estimated, and then the two masks were used as endpoints to prune the tracked bundles. Subsequently, both the target and the dilated homologous ROI were sagittally flipped, and the contralateral tracts were mapped in the pathological hemisphere through the corresponding tracking process (Figure 1: d2, e2).

Comparison between hemispheres.

A numerical quantification of tumor-induced WM damage was assessed by counting the estimated fiber tracts of interest in each hemisphere. The percentage of decrease in tracts was computed for each patient, taking as reference the tracts found in the healthy hemisphere. Moreover, for each case, the tumor volume was computed from the lesion mask previously mentioned and the voxel size (Table 1). In order to investigate the relation between the severity of tumor-induced damages and lesion-specific histological features, a simple linear regression was performed. In particular, for each case we weighed the percentage of tracts decrease by dividing tracts computed value by individual patient's estimated tumor size, in order to account for the relation between amount of disruption and extension of the lesion. Next, we studied the correlation between tracts disruption and MIB1 indexes. Finally, for each patient, reconstructed trajectories were shown in 3D rendered brain to better display the spatial relationship between WM tracts and lesion.

Probabilistic Tractography.

To verify whether the proposed technique accurately obtained all the WM connections and to obtain a measure describing the confidence of the reconstructed trajectories, in every patient, the pathways under examination in the two hemispheres were also defined in a probabilistic framework. In particular, we prepared a parametric model of uncertainty, computing a probability density function (PDF) of the diffusion orientations in each voxel for the multi-fiber population cases, according to the PAS reconstruction approach. Tractography was achieved by iterative streamline propagation through the computed PDFs for each PD estimated, using 1000 iterations. The same tracking procedure was adopted, seeding everywhere in the brain volume and subsequently identifying streamlines connecting the ROIs. For each subject, all tracked individual pathways were combined into a single connection probability image, where each voxel contains the number of streamlines that enter the voxel divided by the total number of streamlines in the input. Within patients, probabilistic and deterministic reconstructed tract volumes were visually compared in each hemisphere as well as between hemispheres, overlaying the two outputs on the same slices. For probabilistic tractography, voxels with the highest connectivity were considered those most likely to be part of the connecting bundles of interest (Figure 1: f1, f2).

Results

Mapping the WM bundles of interest in the pathological hemisphere, after assessing them in the contralateral unaffected one, revealed different types of WM involvement by brain tumors which strongly correlated with the histopathological features of the lesions. Table 1 summarizes the alterations of fiber tracts, as well as some clinical and anatomical data concerning the patients. The higher the MIB-1 label was, the more fibers were found to have been destroyed,

with a correlation coefficient equal to 0.83 (p=0.0001), as shown in Figure 2.

Meningiomas

In patients M1 and M2, the fiber pathway depicted in the healthy hemisphere were found to be splayed into different branches in the affected hemisphere as a result of the tumor mass (Figure 3). Nevertheless, the tractography output showed a peripheral region of intact white matter at tumor boundary where the fiber tracts were still identifiable. Indeed, in the pathological hemisphere, the streamline algorithm did not find under-threshold anisotropy areas, and it reconstructed the connection pathway under examination. This was confirmed by comparing the counts of the estimated fiber tracts in both hemispheres. Most (over two-thirds) of the connecting streamlines identified in the healthy hemisphere were tracked also in the lesioned hemisphere (Table 1).

In the other three cases, deterministic tractography clearly suggested bulk displacement of WM tracts associated with tumor (Figure 3). The lesion mass changed the location and organization of WM pathways but only slightly affected the coherence of fiber bundles. Indeed, in all these cases, meningioma caused a modest decrease in the number of estimated fiber tracts in the lesioned hemisphere, as compared to the healthy WM architecture (Table 1). This indicates that the underlying axonal structures have remained intact but spatially displaced.

This group of patients maintained a degree of connectivity sufficiently comparable to the contralateral hemisphere. Brain tumors like meningiomas do not usually infiltrate the surrounding brain tissue, but simply compress or distort it. The average (± standard deviation [SD]) percent difference in the number of estimated tracts between the two hemispheres across the 5 cases of meningioma was 17.75 ± 9.16 %.

Gliomas

Low-Grade: In patient LGG1, two main connecting fiber bundles were tracked in the healthy WM architecture. The superior bundle reconstructed in the homologous region resulted as being dorsally displaced in the pathological hemisphere. Moreover, the inferior pathway was not identified at all in the lesioned area, probably as a result of tumor-induced destruction. Case LGG5 showed clear displacement of the WM pattern under consideration, as well. The tumor mass destroyed a large part of the fiber tracts and deviated the few that remained intact. In patient LGG3, the inferior pathway that connected the homologous region to the target ROI did not have a contralateral correspondent in the lesioned area. The number of fibers in the other main bundle identified in the healthy hemisphere was notably reduced in the proximity of the tumor. In all the other cases (Cases LGG2, LGG4, LGG6, and LGG7), the tractography outputs showed that glioma did not change the location of the connecting pathway but lead to a reduction in the number of tracts that could not be tracked in the lesioned hemisphere (Figure 4).

The comparative number of estimated fiber tracts in the connection pathways studied was noticeably reduced as compared to contralateral WM architecture (Table 1). Across these seven cases of glioma, the average (±SD) percentage of tract reduction due to tumor infiltration resulted as being 61.9 ± 28.05%, taking into account the high variability in their malignancy.

High-Grade: Evidence of white matter tract infiltration was seen in all four patients with high-grade glioma (HGG #1-4). The fiber bundles estimated in the affected hemisphere were extremely reduced, as compared to the tracts connecting the homologous area and the target ROI of the contralateral hemisphere (Table 1). Tractography results clearly demonstrated this loss of fibers with no displacement of white matter architecture, which is suggestive of tumor invasion (Figure 5). In all four cases, an average (±SD) percent decrease in tracts equal to 93.53 ± 2.78%

was found, taking each patient's non-affected brain hemisphere architecture as a reference.

The difference in percentage between the two main groups (meningiomas and gliomas) of lesion-induced decrease in tracts was statistically significant (p=0.0006). The connection pathways as assessed by using probabilistic tractography confirmed the WM alteration patterns identified in each patient. The connectivity architecture studied by the probabilistic approach mostly corresponded to deterministic tracking outputs previously obtained. In every patients the two types of connection images substantially coincided and no outlier from deterministic tracking were found indicating that the deterministic choice did not compromise the quality of the results. Three exemplificative cases of the qualitative comparisons between the two approaches are reported in Figure 6.

Discussion

In this study, we present a novel approach for defining alterations in WM paths induced by brain lesions by using diffusion tractography. Our method does not take into account anatomically pre-defined fiber tracts, and hence no a priori knowledge of the pathways under investigation is required.

In the proposed approach, the adoption of PAS-MRI as direction reconstruction method for multi-fiber deterministic tractography, reduced the classic limitation of the diffusion tensor model and its inability to differentiate tracts in cases of WM fiber crossing, branching or fanning. Our choice overcame the underestimation of the extent of tracks of interest that may bring to unreliable and clinically misleading information[48], although in a clinically feasible acquisition time.

The results for meningioma show displacements of the WM pathways, indicating the presence of

intact but spatially deviated axonal structures, as previously reported in literature[49,50]. In patients with low-grade glioma, a mixed pattern of tract deviation and disruption was seen, consistently with previous studies[51,52]. All the analyzed cases share a common feature. Low-grade gliomas are usually characterized by an extensive, diffuse infiltration of cancer cells that preferentially invade along myelinated fibers in white matter tracts. The mass effect of the lesion bulk appeared to be insufficient to account for this reduction in fiber tracts, which should most likely be considered as an index of WM disruption caused by tissue infiltration. In the presence of high-grade glioma, tractography was characterized by an almost complete disruption of the fiber bundles[53,54].

Our method used the percentage of decrease in tracts as an effective measure of the severity of WM alterations caused by the tumor mass. The results correlated with histopathological tumoral features. Indeed, our data presented significantly different degrees of WM involvement between the two groups of patients, those with glioma and those with meningioma. In addition, a strong correlation was found between the quantity of fibers disrupted and the MIB-1 index.

The technique we proposed here adopted deterministic tractography for both speed and simplicity of use. Nevertheless, probabilistic tracking is an optimal method for modeling uncertainty, generating multiple curves from a seed point. This method ensures a greater robustness to the image noise[33].

By repeating the comparative tractography analysis in a further probabilistic framework, we were able to confirm the tracking results with a statistical approach. This step of the analysis was so time-consuming (requiring several days for each case) that it could not be applied in a preoperative clinical routine setting, but in this specific case gave us a measure of the reliability of the reconstructed WM pathways. The results of probabilistic tractography further supported the assessment of differences in various types of tumors by observing WM pathway changes, suggesting the feasibility of the proposed method in those critical cases in which the lesion does not involve major/known WM paths and the *a priori* information about the local fibers' anatomy

305 is lacking.

306 Limitations of the Study

307 We are aware that our work is based on a relatively small sample size. Nonetheless, the results
308 obtained and they congruence in the various patients belonging to the three main classes of
309 tumors, suggest stereotypical tumor-induced WM alterations, in relation to the type and the
310 severity of the lesion.

311 Two different strategies were followed in defining the tracts of interest for the comparative
312 tracking analysis, depending on the number of selected target ROIs, subjectively chosen, case-by-
313 case. This approach was forced by the heterogeneity of our cohort of patients that presented
314 different lesion location and size. However, it didn't affect the validity of data since all the
315 analysis were conducted within subject, between the two hemispheres.

316 All the analyzed cases were patients who underwent awake surgery at the Department of
317 Neurosurgery of the University Hospital Santa Maria della Misericordia of Udine. The surgical
318 procedures were conducted under intraoperative cortical (and occasionally subcortical) electrical
319 stimulation for localizing functional areas prior to neurosurgical resection of brain tumors
320 invading, or close to, eloquent brain regions[55]. In the present work we didn't take into account
321 these data since we were interested in performing a novel data-driven tracking approach without
322 any Navigated Brain Stimulation-guided tract reconstruction.

323 We used five software packages to analyze our data. This was our own choice, since we
324 decided to adopt specialized algorithms specific of the packages, instead of following a single
325 work-flow. In view of a clinical routine, a uniform interface that combines all the processing
326 steps within a single framework would be useful.

327 Multi-shot echo-planar imaging (EPI) was adopted. This achieve higher spatial resolution
328 to fully capture the complex axonal configurations and limitate the partial volume effects

enhanced from the anisotropic-voxel acquisition performed, at the expense of more susceptiblity to motion.

HARD tractography methods, such as the one we used, greatly improved resolution for detecting crossing fibers, but are still susceptible to errors introduced by uncertainty at sites of fiber crossing. This is typical of any deterministic tractography analysis especially with T2-weighted signal abnormalities in the proximity or within the lesion. Nevertheless, we attempted to minimize this confound by introducing a complementary probabilistic framework.

Conclusion

Diffusion imaging has become an essential part of MRI examinations in brain tumor patients. To date, diffusion tractography is the only imaging technique able to provide spatial maps of WM pathways in vivo. Our method suggests that analysis of connectivity can be used to complement fractional anisotropy in clinical studies as it might reveal other features, like the deviation or disruption of fiber tracts, and correlates well with the lesion histopathology. The proposed method is able to best exploit streamline tractography and may represent a possible preoperative diagnostic technique. Moreover, the inspection of the results can help in identifying WM tracts particularly important for brain functionality. Involvement of white matter fibers represents an important piece of information to correctly plan the surgical approach and to evaluate the extent of a safe resection in patients with intrinsic brain tumors. Further research is however needed to fully assess the clinical relevance of this approach.

Conflict of Interest

The authors declare no competing financial interests.

References

1. Field AS, Alexander AL, Wu YC, Hasan KM, Witwer B, Badie B. Diffusion Tensor Eigenvector Directional Color Imaging Patterns in the Evaluation of Cerebral White Matter Tracts Altered by Tumor. J Magn Reson Imaging 2004; 20: 555-562.

2. Jellison BJ, Field AS, Medow J, Lazar M, Salamat MS, Alexan-der AL. Diffusion Tensor Imaging of Cerebral White Matter:A Pictorial Review of Physics, Fiber Tract Anatomy, and Tumor Imaging Patterns. AJNR Am J Neuroradiol 2004; 25: 356-369.

3. Skrap M, Mondani M, Tomasino B, Weis L, Budai R, Pauletto G, Eleopra R, Fadiga L, Ius T. Surgery of insular nonenhancing gliomas: volumetric analysis of tumoral resection, clinical outcome, and survival in a consecutive series of 66 cases. Neurosurgery 2004; 70(5), 1081-1094.

4. Clark CA, Barrick TR, Murphy MM, Bell BA. 2003. White matter fiber tracking in patients with space-occupying lesions of the brain:a new technique for neurosurgical planning? Neuroimage 2003; 20: 1601-1608.

5. Basser PJ, Mattiello J, Le Bihan D. MR diffusion tensor spectroscopy and imaging. Biophys J 1994; 66:259 –267.

6. Conturo TE, Lori NF, Cull TS, Akbudak E, Snyder AZ, Shimony JS, McKinstry RC, Burton H, Raichle ME. Tracking neuronal fiber pathways in the living human brain. Proc. Natl. Acad. Sci 1999; USAv96: 10422 – 10427.

7. Mori S, Crain BJ, Chacko VP, van Zijl PCM. Three dimensional tracking of axonal projections in the brain by magnetic resonance imaging. Annals of Neurology 1999; 45:265–269.

8. Basser PJ, Pajevic S, Pierpaoli C, Duda J, and Aldroubi A. In vivo fiber tractography using DT-MRI data. Magnetic Resonance in Medicine 2000; 44:625–632.

9. Bertani G, Carrabba G, Raneri F, Fava E, Castellano A, Falini A, Casarotti A, Gaini SM, Bello

L. Predictive value of inferior fronto-occipital fasciculus (IFO) DTI-fiber tracking for determining the extent of resection for surgery of frontal and temporal gliomas preoperatively. J Neurosurg Sci. :2012; 56(2):137-43.

10. Zolal A, Hejčl A, Vachata P, Bartoš R, Humhej I, Malucelli A, Nováková M, Hrach K, Derner M, Sameš M. The use of diffusion tensor images of the corticospinal tract in intrinsic brain tumor surgery: a comparison with direct subcortical stimulation. Neurosurgery 2012; 71(2):331-40.

11 Lazar M, Alexander AL, Thottakara PJ, et al. White matter reorganization after surgical resection of brain tumors and vascular malformations, AJNR Am J Neuroradiol 2006; 27:1258-71.

12. Xu JL, Li YL, Lian JM, Dou SW, Yan FS, Wu H, Shi DP. Distinction between postoperative recurrent glioma and radiation injury using MR diffusion tensor imaging. Neuroradiology 2010; 52(12):1193-9.

13. Kovanlikaya I, Firat Z, Kovanlikaya A, Uluğ AM, Cihangiroglu MM, John M, Bingol CA, Ture U. Assessment of the corticospinal tract alterations before and after resection of brainstem lesions using Diffusion Tensor Imaging (DTI) and tractography at 3T. Eur J Radiol. 2011; 77(3): 383-91.

14. Nowosielski M, Recheis W, Goebel G, Güler O and Tinkhauser G, et al. ADC histograms predict response to anti-angiogenic therapy in patients with recurrent high-grade glioma. Neuroradiology 2011; 53(4): 291-302.

15. Kinoshita M, Hashimoto N, Gogo T, et al. Fractional anisotropy and tumor cell density of the tumor core show positive correlation in diffusion tensor magnetic resonance imaging of malignant brain tumors, NeuroImage 2008; 43:29–35.

16. Byrnes TJ, Barrick TR, Bell BA, Clark CA. Diffusion tensor imaging discriminates between

glioblastoma and cerebral metastases in vivo. NMR Biomed. 2011; 24(1):54-60.

17. Chen Y, Shi Y, Song Z. Differences in the architecture of low-grade and high-grade gliomas evaluated using fiber density index and fractional anisotropy. J Clin Neurosci 2010; 17(7):824-9.

18. Jolapara M, Kesavadas C, Radhakrishnan VV, Thomas B, Gupta AK, Bodhey N, Patro S, Saini J, George U, Sarma PS. Role of diffusion tensor imaging in differentiating subtypes of meningiomas. J Neuroradiol. 2010; 37(5):277-83.

19. Clark CA, Barrick TR, Murphy MM, Bell BA. White matter tracking in patients with space-occupying lesions of the brain: a new technique for neurosurgical planning? NeuroImage 2003; 20: 1601 – 1608.

20. Yamada K, Kizu O, Mori S, Ito H, Nakamura H, Yuen S, Kubota T.Tanaka O, Akada W, Sasajima H, Mineura K, Nishimura T. Brain fiber tracking with clinically feasible diffusion tensor MR imaging: Initial experience. Radiology 2003; 227:295 – 301.

21. Morita N, Wang S, Kadakia P, Chawla S, Poptani H, Melhem ER. Diffusion tensor imaging of the corticospinal tract in patients with brain neoplasms. Magn Reson Med Sci. 2011; 10(4):239-43.

22. Bobek-Billewicz B, Stasik-Pres G, Majchrzak K, Senczenko W, Majchrzak H, Jurkowski M, Połetek J. Fibre integrity and diffusivity of the pyramidal tract and motor cortex within and adjacent to brain tumour in patients with or without neurological deficits. Folia Neuropathol. 2011; 49(4):262-70.

23. Pantelis E, Papadakis N, Verigos K, Stathochristopoulou I, Antypas C, Lekas L, Tzouras A, Georgiou E, Salvaras N. 2010. Integration of functional MRI and white matter tractography in stereotactic radiosurgery clinical practice. Int J Radiat Oncol Biol Phys. 2010; 78(1):257-67.

24. Kleiser R, Staempfli P, Valavanis A, Boesiger P, Kollias S. Impact of fMRI-guided advanced

DTI fiber tracking techniques on their clinical applications in patients with brain tumors. Neuroradiology 2010; 52(1):37-46.

25. Bucci M, Mandelli ML, Berman JI, Amirbekian B, Nguyen C, Berger MS, Henry RG. Quantifying diffusion MRI tractography of the corticospinal tract in brain tumors with deterministic and probabilistic methods. Neuroimage Clin. 2013 Aug 20;3:361-8.

26. Giussani C, Roux FE, Ojemann J, Sganzerla EP, Pirillo D, Papagno C. Is preoperative functional magnetic resonance imaging reliable for language areas mapping in brain tumor surgery? Review of language functional magnetic resonance imaging and direct cortical stimulation correlation studies. Neurosurgery. 2010 Jan;66(1):113-20. doi: 10.1227/01.NEU.0000360392.15450.C9.

27. Peled S, Friman O, Jolesz F, Westin CF. Geometrically constrained two-tensor model for crossing tracts in DWI. Magn Reson Imaging. 2006 Nov;24(9):1263-70. Epub 2006 Sep 12.

28. Tournier JD, Calamante F, Connelly A. Robust determination of the fibre orientation distribution in diffusion MRI: non-negativity constrained super-resolved spherical deconvolution. Neuroimage. 2007 May 1;35(4):1459-72. Epub 2007 Feb 21.

29. Sotiropoulos SN, Bai L, Morgan PS, Auer DP, Constantinescu CS, Tench CR. A regularized two-tensor model fit to low angular resolution diffusion images using basis directions. J Magn Reson Imaging. 2008 Jul;28(1):199-209.

30. Jansons K, Alexander D. Persistent angular structure: new insights from diffusion magnetic resonance imaging data. Inverse Probl. 2003; 19(5):1031 – 1046.

31. Bertani G, Carrabba G, Raneri F, Fava E, Castellano A, Falini A, Casarotti A, Gaini SM, Bello L. Predictive value of inferior fronto-occipital fasciculus (IFO) DTI-fiber tracking for determining the extent of resection for surgery of frontal and temporal gliomas preoperatively. J Neurosurg Sci. :2012; 56(2):137-43.

443 32. Brat DJ, Prayson RA, Ryken TC, Olson J. Diagnosis of malignant glioma: role of
444 neuropathology, J Neurooncol 2008; 89:287–311.
445 33. Behrens TE, Woolrich MW, Jenkinson M, Johansen-Berg H, Nunes RG, Clare S, Matthews
446 PM, Brady JM, Smith SM. Characterization and propagation of uncertainty in diffusion-weighted
447 MR imaging. Magn Reson Med. 2003 Nov;50(5):1077-88.
448 34. Parker GJM, Haroon HA, Wheeler-Kingshott CAM. A framework for a streamline-based
449 probabilistic index of connectivity (PICo) using a structural interpretation of MRI diffusion
450 measurements. J Magn Reson Imaging 2003;18:242-54.
451 35. Louis DN, Ohgaki H, Wiestler OD, Cavenee WK, Burger PC, Jouvet A, Scheithauer BW,
452 Kleihues P. The 2007 WHO Classification of Tumours of the Central Nervous System
453 Acta Neuropathol 2007 Aug;114(2):97-109. Epub 2007 Jul 6.
454 36. Cook PA, Bai Y, Nedjati-Gilani S, Seunarine KK, Hall MG, Parker GJ, Alexander DC,
455 Camino: Open-Source Diffusion-MRI Reconstruction and Processing, 14th Scientific Meeting of
456 the International Society for Magnetic Resonance in Medicin, Seattle, WA, USA, p. 2759,
457 May 2006.
458 37. Smith SM, Jenkinson M, Woolrich MW, Beckmann CF, Behrens TEJ, Johansen-Berg H,
459 Bannister PR, De Luca M, Drobnjak I, Flitney DE, Niazy R, Saunders J, Vickers J, Zhang Y, De
460 Stefano N, Brady JM, Matthews PM, Advances in functional and structural MR image analysis
461 and implementation as FSL. NeuroImage 2004; 23(S1):208-219.
462 38. Cox RW. AFNI: software for analysis and visualization of functional magnetic resonance
463 neuroimages. Comput Biomed Res. 1996; 600: 29:162-173.
464 39. Yushkevich PA, Piven J, Hazlett HC, Smith RG, Ho S, Gee JC, Gerig G. User-guided 3D
465 active contour segmentation of anatomical structures: Significantly improved efficiency and
466 reliability. Neuroimage 2006; 1; 31(3):1116-28.

467 40. Smith SM. Fast robust automated brain extraction, Hum Brain Mapp 2002; 17:143-155.

468 41. Jenkinson M, Smith SM. A global optimisation method for robust affine registration of brain
469 images. Medical Image Analysis, 5(2):143-156, 2001.

470 42. Seunarine K, Cook P, Hall M, Embleton K, Parker G, Alexander D. Exploiting peak
471 anisotropy for tracking through complex structures. IEEE ICCV Workshop on MMBIA, 2007.

472 43. Sweet and Alexander , Reduced Encoding Persistent Angular Structure, 572 ISMRM, 2010.

473 44. Ashburner J, Friston KJ. Unified segmentation. Neuroimage 2005; 26:839-851.

474 45. Mori S, Crain BJ, Chacko VP, van Zijl PCM. Three-dimensional tracking of axonal
475 projections in the brain by magnetic resonance imaging, Annals of Neurology 1999; 45:265-269.

476 46. Thiebaut de Schotten M, Ffytche DH, Bizzi A, Dell'Acqua F, Allin M, Walshe M, Murray R,
477 Williams SC, Murphy DG, Catani M. Atlasing location, asymmetry and inter-subject variability
478 of white matter tracts in the human brain with MR diffusion tractography. Neuroimage. 2011 Jan
479 1;54(1):49-59.

480 47. Campanella M, Molinari E, Baraldi P, Nocetti L, Porro CA, Alexander DC. An algorithm to
481 estimate anatomical connectivity between brain regions using diffusion MRI, MRI 2012: Volume
482 31, Issue 32.

483 48. Farquharson S, Tournier JD, Calamante F, Fabinyi G, Schneider-Kolsky M, Jackson GD,
484 Connelly. White matter fiber tractography: why we need to move beyond DTI. A.J Neurosurg.
485 2013 Jun;118(6):1367-77. doi: 10.3171/2013.2.JNS121294. Epub 2013 Mar 29.

486 49. Corie W. Wei, Gang Guo, David J. MikulisTumor Effects on Cerebral White Matter as
487 Characterized by Diffusion TensorTractography, Can. J. Neurol. Sci. 2007; 34: 62-69

488 50. Carvi y Nievas MN, Hoellerhage HG, Drahten C. White matter tract alterations assessed with
489 diffusion tensor imaging and tractography in patients with solid posterior fossa tumors. Neurol

India 2010;58:914-21

51. Kuhnt D, Bauer MH, Egger J, Richter M, Kapur T, Sommer J, Merhof D, Nimsky CFiber tractography based on diffusion tensor imaging compared with high-angular-resolution diffusion imaging with compressed sensing: initial experience. Neurosurgery. 2013 Jan;72 Suppl 1:165-75. doi: 10.1227/NEU.0b013e318270d9fb.

52. Castellano A, Bello L, Michelozzi C, Gallucci M, Fava E, Iadanza A, Riva M, Casaceli G, Falini A, Role of diffusion tensor magnetic resonance tractography in predicting the extent of resection in glioma surgery. Neuro Oncol. 2012 Feb;14(2):192-202. doi: 10.1093/neuonc/nor188. Epub 2011 Oct 20

53. Gulati S, Berntsen EM, Solheim O, Kvistad KA, Håberg A, Selbekk T, Torp SH, Unsgaard G.Minim. Surgical resection of high-grade gliomas in eloquent regions guided by blood oxygenation level dependent functional magnetic resonance imaging, diffusion tensor tractography, and intraoperative navigated 3D ultrasound. Invasive Neurosurg. 2009 Feb; 52(1):17-24. doi: 10.1055/s-0028-1104566. Epub 2009 Feb 26

54. Chen F, Zhang X, Li M, Wang R, Wang HT, Zhu F, Lu DJ, Zhao H, Li JW, Xu Y, Zhu B, Zhang B, Axial diffusivity and tensor shape as early markers to assess cerebral white matter damage caused by brain tumors using quantitative diffusion tensor tractography. CNS Neurosci Ther. 2012 Aug;18(8):667-73. doi: 10.1111/j.1755-5949.2012.00354.x. Epub 2012 Jun 19.

Figure 1

Figure 1: Method schematics

(a) 3D tumor ROI was identified from the anatomical MRI image.
(b) The ROI was mirrored across the sagittal mid-plane to obtain the homologous region in the healthy hemisphere. A segmentation was performed and the intersection between the flipped tumor ROI and the white matter mask was computed; (c) The intersection mask was then transformed from the structural to the native diffusion space and used as the “seed” in the deterministic tractography analysis. Streamlines were generated from every point within the seed mask in the healthy hemisphere and two (d1) or only one (d2) target regions were identified; (e1) In the first case the WM bundles connecting the two target ROIs were investigated. The targets were sagittally mirrored and, after seeding, the tracts of interest in the lesioned hemisphere were generated in the same manner. (e2) In the second case the homologous region mask was dilated and the streamlines connecting the dilated ROI and the target were tracked to estimate the contralateral WM tracts involved in the tumor area. Subsequently, both the target and the dilated homologous ROI were sagittally flipped and the contralateral tracts were reconstructed in the pathological hemisphere; (e1)-(e2) The tracts of interest in the two hemispheres were finally defined in a probabilistic framework following the same tracking procedures and according to the number of targets identified. Single connection probability images were thus obtained to confirm deterministic tracking results.

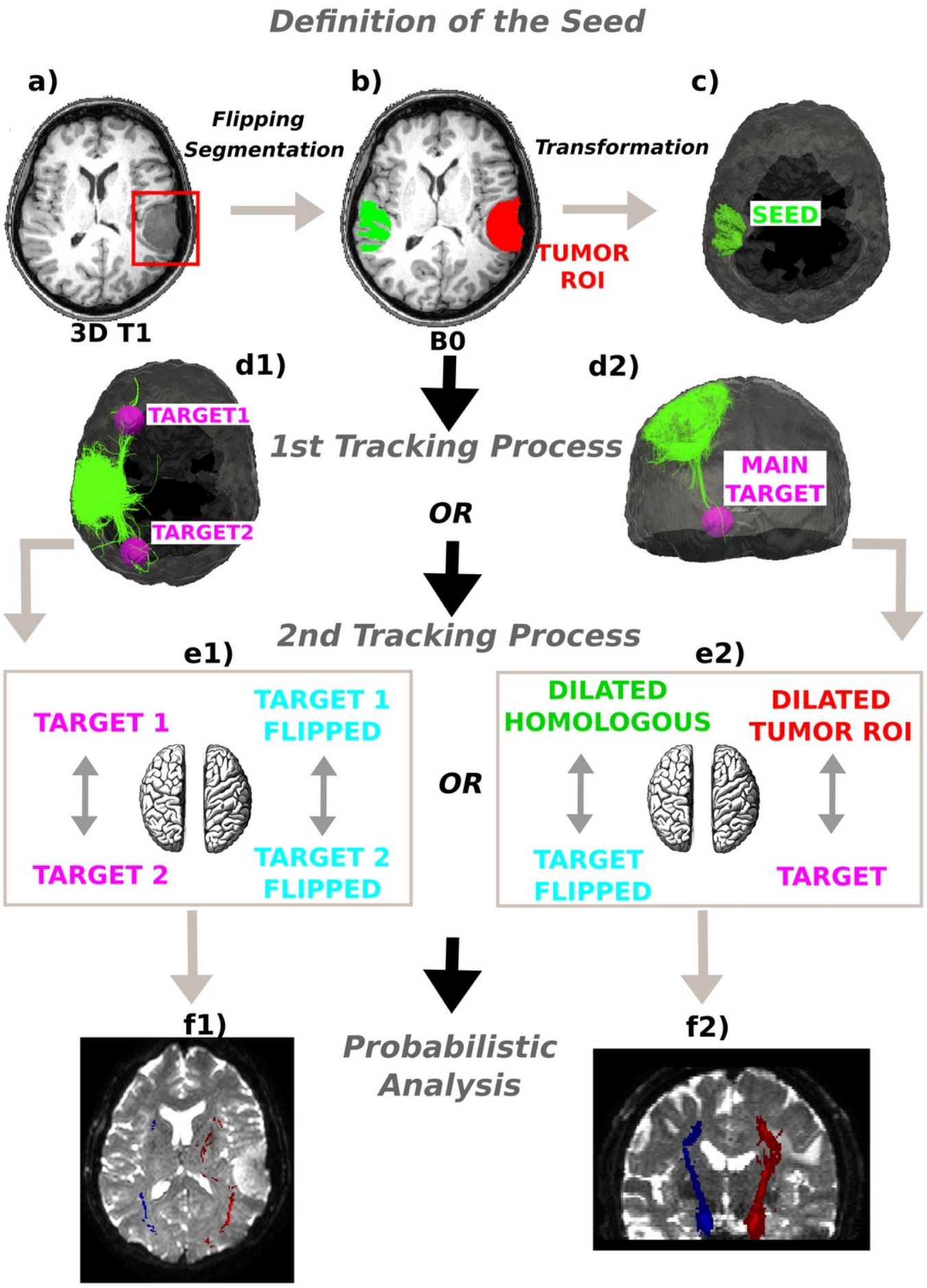

Figure 2

Figure 2

Linear regression between the pondered tumor-induced reductions in tracts and lesion-specific histological features (MIB-1 index) across all the studied cases; scatter plot shows the data and the estimated linear fitting.

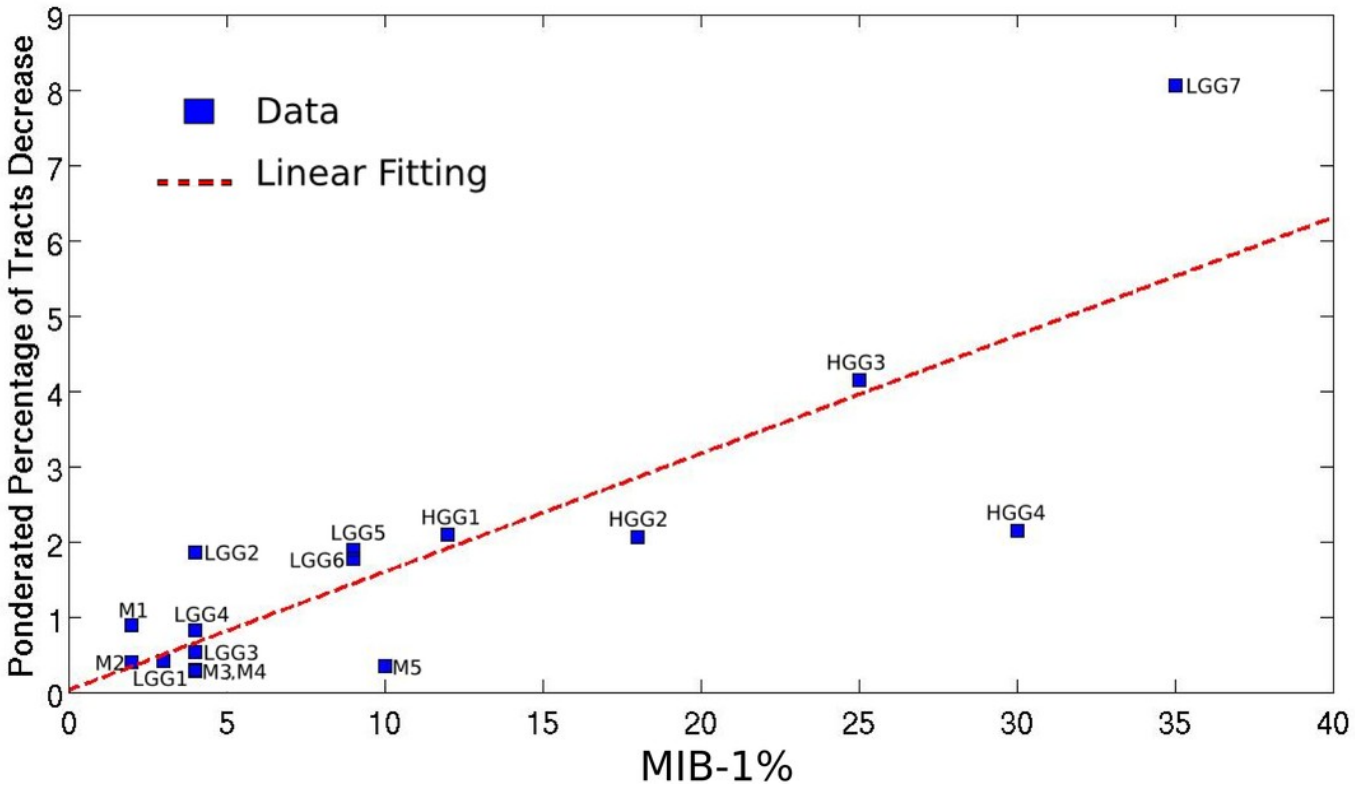

Figure 3

Figure 3 : Comparative tractography study between the two hemispheres in the five cases of meningioma.

Cases M1, M2 and M5: Estimation of the fiber tracts between the main target and the dilated region homologous to the tumor in the healthy hemisphere; comparison with the contralateral lesioned architecture. In the case M1 the ascending fibers from the thalamus to cerebral cortex and the descending fibers from the fronto-parietal cortex to subcortical nuclei and spinal cord were splayed into different branches in the lesioned hemisphere. The same alteration pattern was identified in the cortico-ponto-cerebellar tract reconstructed in patient M2, as a result of the tumor mass. The fiber tracts that leave the internal capsule ventrally and continue into the cerebral peduncles, pons and piramidal tract in the pathological hemispehere of patient M5 resulted bulky displaced, in relation to the contralateral WM architecture. Cases M3 and M4: Estimation of the fiber tracts between the two target regions in the healthy hemisphere, and comparison with the contralateral lesioned architecture. The lesion mass changed the location and organization of the inferior fronto-occipital fasciculus tracked in the healthy hemisphere in both patients M3 and M4.

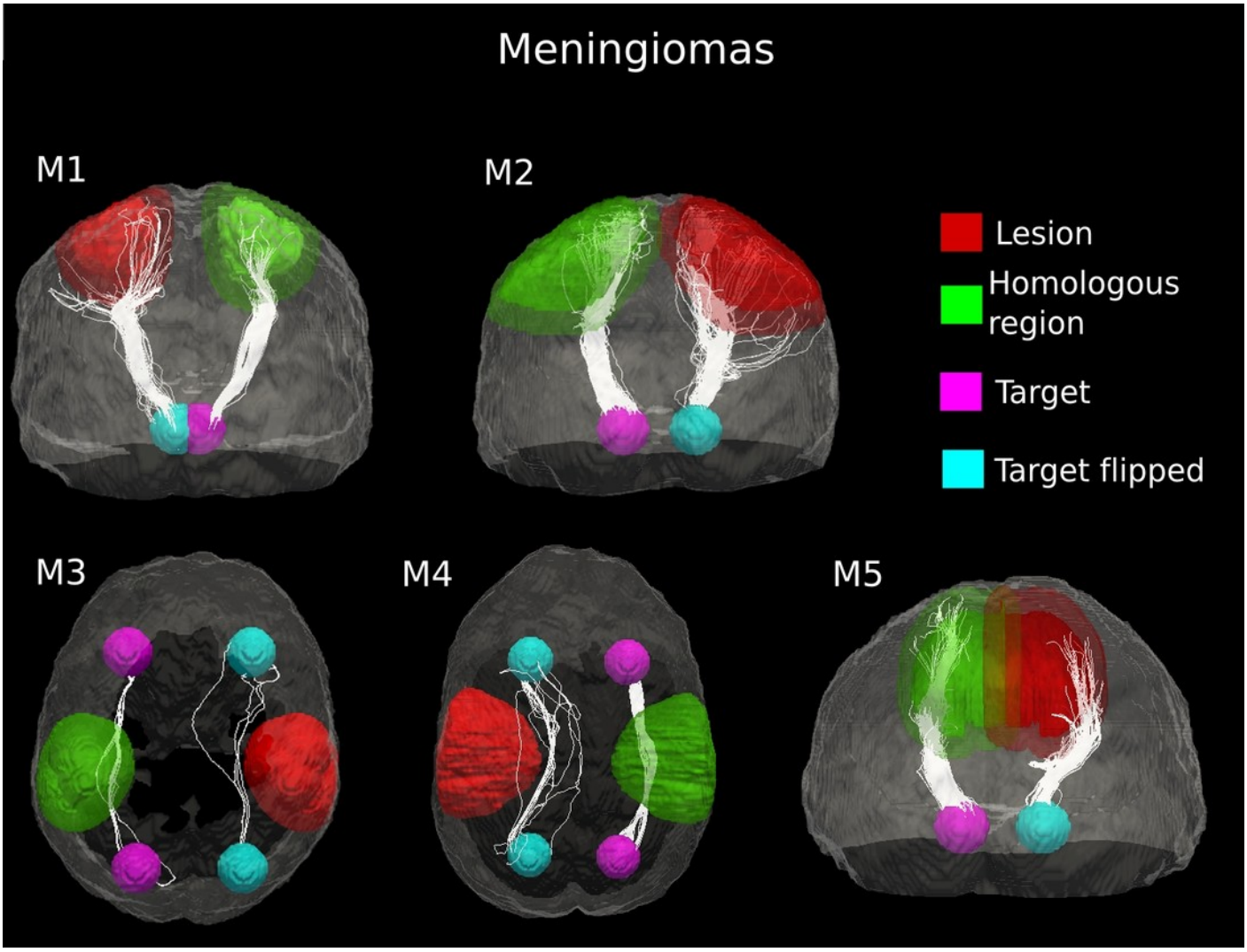

Figure 4

Figure 4: Comparative tractography study between the two hemispheres in the seven cases of low-grade glioma.

Cases LGG1 and LGG5: Estimation of the fiber tracts between the two target regions in the healthy hemisphere, and comparison with the contralateral affected architecture. The superior bundle of Cingulum, reconstructed in the homologous region, resulted dorsally displaced in the pathological hemisphere in case LGG1, while its inferior pathway was not identified at all in the lesioned area. The inferior Fronto-Occipital Fasciculus, tracked in patient LGG5, was displaced as well.

Cases LGG2, LGG3, LGG4, LGG6, and LGG7: estimation of the fiber tracts between the main target and the dilated region homologous to the tumor in the healthy hemisphere; comparison with the contralateral affected architecture. The Superior Longitudinal Fascicle identified in case LGG2 could not be tracked in the affected hemisphere. In patient LGG3, the inferior bundle of the Arcuate Fasciculus that connected the homologous region to the target ROI resulted destroyed in the pathological area. The Cerebellar tracts tracked in patients LGG4 and LGG6 appeared disrupted by the infiltrating tumor mass. Finally, in patient LGG7 the inferior part of Arcuate fasciculus, reconstructed in the healthy hemisphere resulted mostly destroyed in the contralateral area.

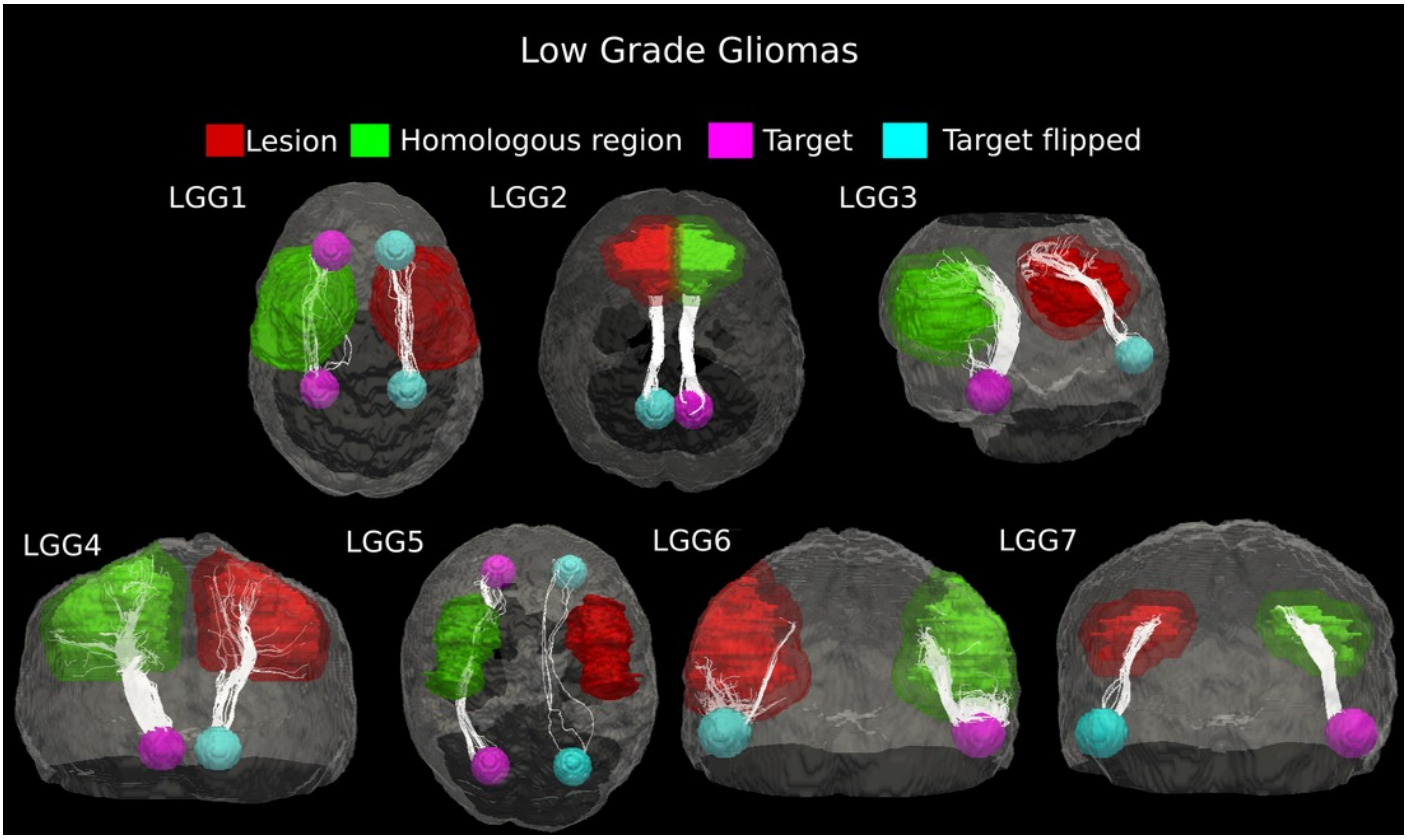

Figure 5

Figure 5: Comparative tractography study between the two hemispheres in the four cases of high-grade glioma.

Cases HGG1, HGG2, HGG3, and HGG4: estimation of the fiber tracts between the main target and the dilated region homologous to the tumor in the healthy hemisphere; comparison with the contralateral lesioned architecture. Tumor infiltration can be clearly seen in all the four cases. The Superior Longitudinal Fascicle in the affected hemisphere was largely disrupted in both patients HGG1 and HGG3. The Arcuate Fasciculus connecting the homologous area and the target ROI in the healthy hemisphere of case HGG2, resulted almost entirely destroyed in the tumor area. In addition, tractography in patient HGG4 demonstrated the huge loss of fiber tracts belonging to the Inferior Fronto-Occipital Fasciculus and the Cingulum reconstructed in the healthy brain contralateral area.

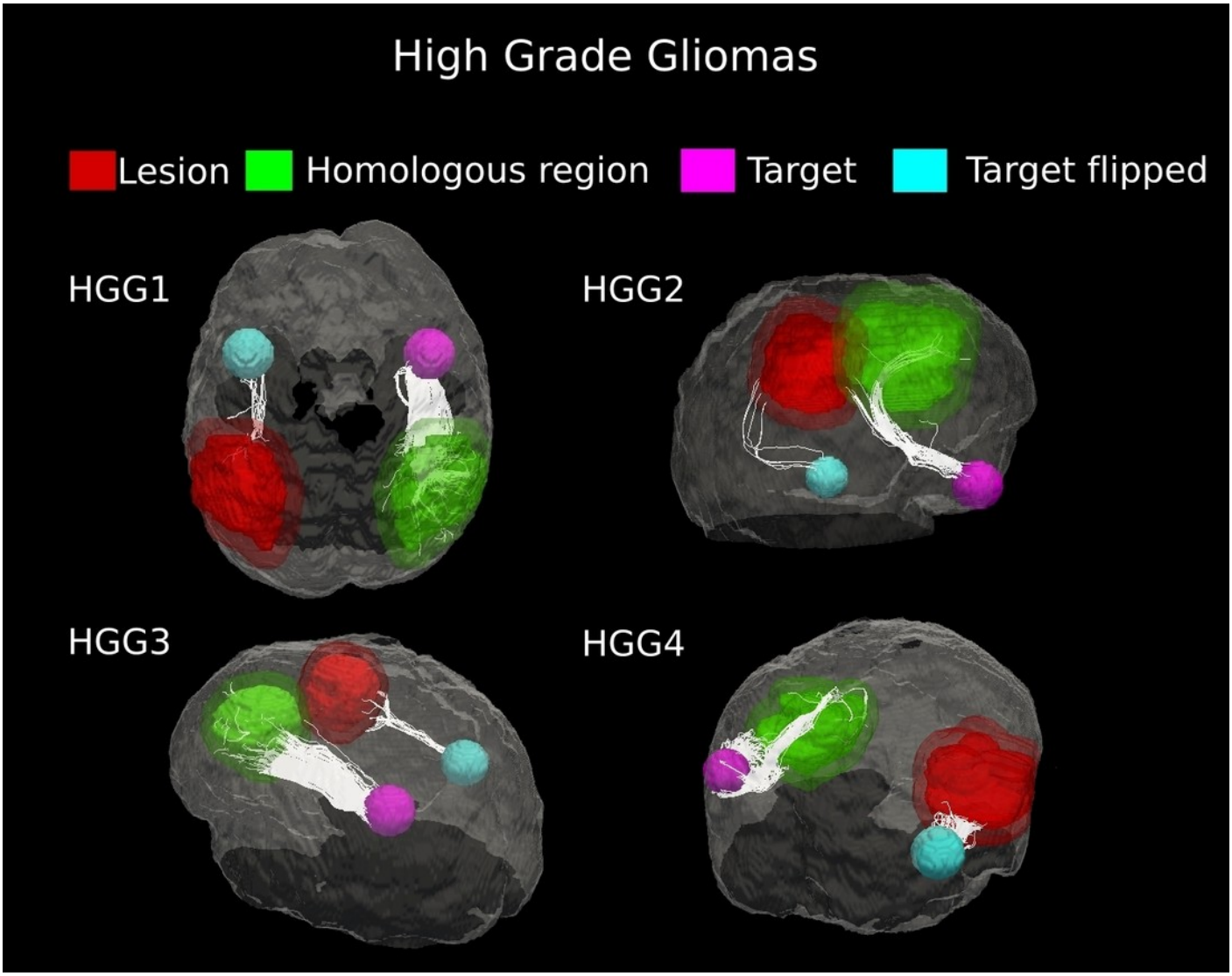

Figure 6

Figure 6: Connection probability maps in the two hemispheres for three exemplificative cases.

(Meningioma M3; Low-Grade Glioma LGG4; High-Grade Glioma HGG3). The probability maps, in which each voxel value corresponds to the number of streamlines that enter the voxel divided by the total number of streamlines in the input, are overlaid onto coronal and axial views of the b0 brain volume. Results showed different degrees of severity in the tumor-induced alterations of white matter tracts, as compared to the contralateral architecture. On the left and right sides, connectivity maps obtained by deterministic tractography confirm that the deterministic algorithm tracked all the important connections shown by the probabilistic analysis.

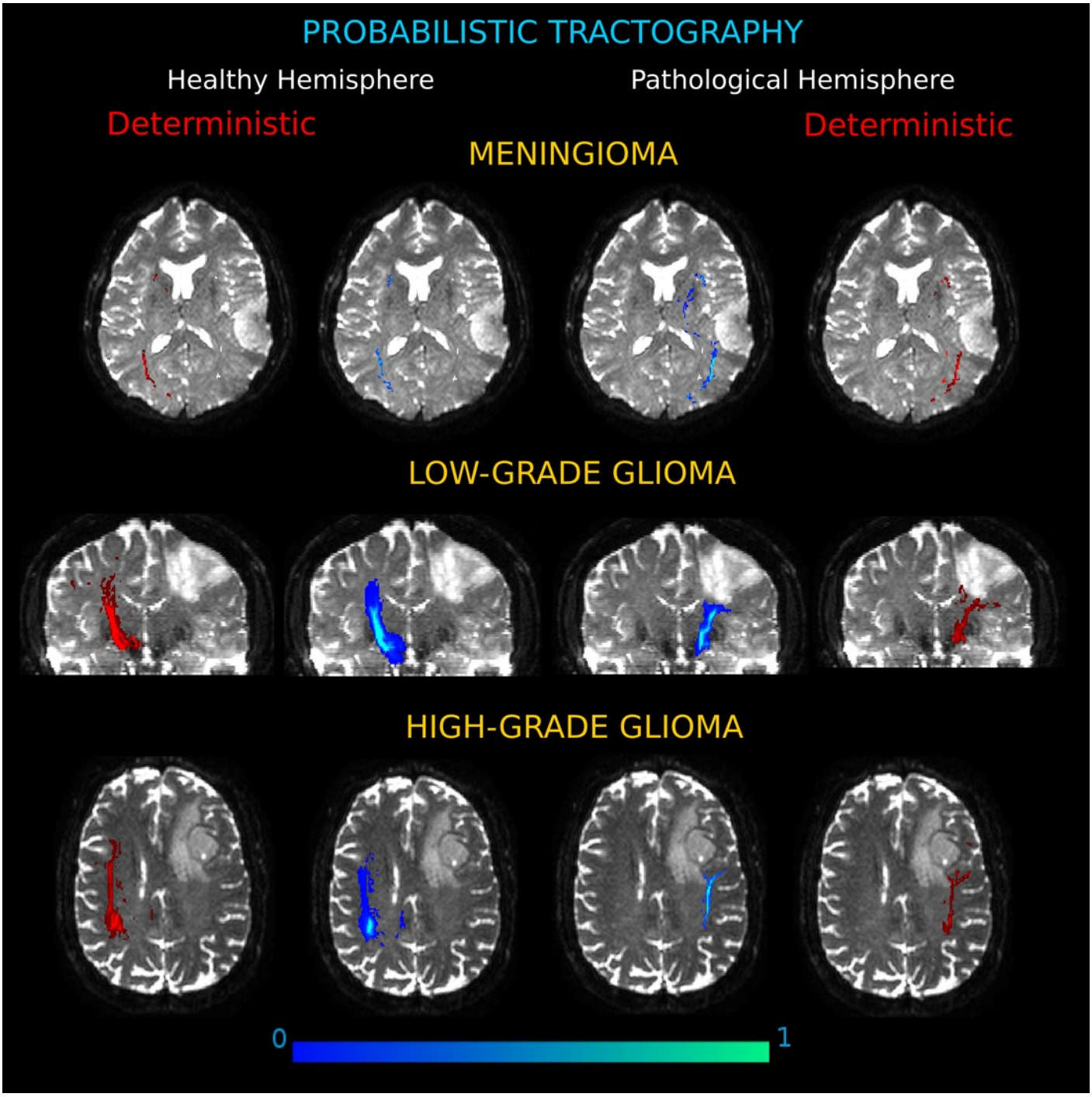

Table 1(on next page)

Table 1

Clinical information and outcomes in the cohort of patients.

Case No.	Age(yrs)	Sex	Tumor Location	Tumor Size [cm3]	Mib-1%	Percentage Decrease in Tract Count
MENINGIOMA						
M1	68	M	RH Premotor Motor	11.67	2	10.41%
M2	55	M	LH Parietal Motor	52.99	2	21.25%
M3	48	F	LH Temporal Parietal Motor	36.16	4	10.00%
M4	27	F	RH Temporal Motor Premotor	106.25	4	32.00%
M5	35	M	LH Premotor Motor	43.03	10	15.10%
LOW GRADE GLIOMA						
LGG1	28	F	LH Insular Temporal	107.4	3	45.10%
LGG2	37	F	RH Frontal	13.29	4	24.68%
LGG3	37	F	LH Frontal Premotor	53.38	4	28.72%
LGG4	38	M	LH Frontal Premotor	98.83	4	81.25%
LGG5	46	M	LH Temporal Occipital Insular	43.2	9	81.81%
LGG6	50	M	RH Insular Temporal Parietal	46.15	9	81.85%
LGG7	40	M	RH Premotor	11.16	35	89.92%
HIGH GRADE GLIOMA						
HGG1	41	F	RH Temporal Motor Parietal	45.53	12	95.58%
HGG2	51	F	RH Frontal PremotorMotor	46.62	18	96.18%
HGG3	32	M	LH Frontal Premotor	21.8	25	90.43%
HGG4	49	M	LH Premotor Motor Insular	43.02	30	91.95%

Table 1: *Clinical information and outcomes in the cohort of patients.*